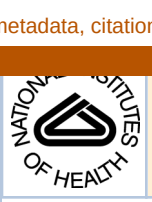

Published in final edited form as:

Adv Mater. 2011 March 25; 23(12): H79–H83. doi:10.1002/adma.201004333.

Synthesis of Size-tunable Polymeric Nanoparticles Enabled by 3D Hydrodynamic Flow Focusing in Single-Layer Microchannels

Minsoung Rhee[†],
Department of Mechanical Engineering Massachusetts Institute of Technology, Cambridge, MA 02139

David H. Koch Institute for Integrative Cancer Research Massachusetts Institute of Technology, Cambridge, MA 02139

Pedro M. Valencia[†],
Department of Chemical Engineering Massachusetts Institute of Technology, Cambridge, MA 02139

Maria I. Rodriguez,
Department of Electrical Engineering and Computer Science Massachusetts Institute of Technology, Cambridge, MA 02139

Robert Langer,
David H. Koch Institute for Integrative Cancer Research Massachusetts Institute of Technology, Cambridge, MA 02139

Department of Chemical Engineering Massachusetts Institute of Technology, Cambridge, MA 02139

Omid C. Farokhzad, and
Laboratory of Nanomedicine and Biomaterials Department of Anesthesiology, Brigham and Women's Hospital Harvard Medical School, Boston, MA 02115

Rohit Karnik
Department of Mechanical Engineering Massachusetts Institute of Technology, Cambridge, MA 02139

Laboratory of Nanomedicine and Biomaterials Department of Anesthesiology, Brigham and Women's Hospital Harvard Medical School, Boston, MA 02115

Keywords

Polymeric Nanoparticles; PLGA-PEG; Nanoprecipitation; 3D Hydrodynamic Focusing; Microfluidic

Recently, polymeric nanoparticles (NPs) have attracted enormous attention as targeted drug delivery vehicles.[1-4] Especially, biodegradable and biocompatible polymeric NPs comprised of poly(lactide-*co*-glycolide)-*b*-polyethyleneglycol (PLGA-PEG) block copolymers exhibit optimal physicochemical characteristics such as the ability to incorporate various targeting agents, enhanced immune evasion, controlled drug release, and

Correspondence to: Omid C. Farokhzad; Rohit Karnik.

karnik@mit.edu ofarokhzad@zeus.bwh.harvard.edu.

[†]These authors contributed equally to the paper.

Supporting Information Supporting Information is available online from Wiley InterScience or from the author.

high payload of drug molecules.[5-6] Targeted PLGA-PEG NPs have shown very promising *in vivo* results for treatment of cancer[7-9] and they are now poised to enter clinical trials. Preparation of such targeted NPs in a robust and reproducible manner has thus become very important for therapeutic applications where precise control of the physicochemical properties of NPs is required to achieve optimal biodistribution and therapeutic efficacy.[10]

While the conventional approach to synthesize polymeric NPs relies on 'bulk' nanoprecipitation by solvent exchange,[11-12] our group recently reported a new reproducible synthesis of highly uniform PLGA-PEG NPs using 2D hydrodynamic flow focusing (HFF) in microfluidic channels.[13-14] In this method, the polymer stream in acetonitrile (ACN) horizontally focused only by water sheath streams experiences rapid mixing with water with a characteristic mixing time faster than the NP assembly time, resulting in homogeneous NPs.[13,15] However, one of the challenges for optimal NP synthesis by 2D HFF is that NPs made from polymers with a PLGA block of high molecular weight (MW) (> 45 kDa) tend to aggregate on the channel walls, resulting in clogging of the channels. Aggregation is caused by the adsorption of the hydrophobic PLGA onto the hydrophobic walls of PDMS, which depends both on concentration and molecular weight.[16-17] This substantially reduces the robustness of operation – the ability to synthesize NPs without device failure – and is a nontrivial drawback of the 2D HFF technique because NPs made from high MW PLGA blocks tend to exhibit higher drug loading and tunable drug release profile as the polymer MW is varied.[12,18-19] Furthermore, aggregation of the polymer on the channel walls frequently causes the device to irreversibly fail due to increased internal pressure.[20] Such channel fouling may be circumvented by modification of the channel surface with Teflon-like materials.[21] However, efficient surface modification requires laborious silicon/glass fabrication or a separate deposition/curing step that is extremely demanding, and the coating tends to degrade over time. For this application and many others, a preferred solution would be to isolate the precipitating polymer from the channel walls by 3D focusing in both the horizontal and the vertical dimensions, thereby preventing aggregation and clogging. Over the past few years, several unique 3D HFF systems have been reported,[22-31] including intrinsic 3D structures such as horizontal nozzles[22-23] and vertical chimneys[24]. Other 3D HFF systems with 3D channel network either with a single two-level layer[27-28] or with two individual layers[29-31] have been also proposed. However, their construction requires high-level expertise of fabrication, considerably high costs and limited reproducibility. More recently, 'microfluidic drifting,' a methodology of 3D fluid manipulation in a single layer, has been also introduced.[25-26] Despite its fabrication simplicity, this method functions only at high *Re* numbers and a relatively low sample flow rate, which may cause substantial dilution of the sample flow and low throughput. Because of the complications with the previously proposed 3D HFF systems, there is demand for a platform that is sufficiently versatile and simple for both fabrication and operation.

In this paper we present a simple design for 3D HFF composed of a monolithic single layer with three sequential inlets for vertical focusing followed by a conventional cross junction for horizontal focusing. We use this device for the synthesis of polymeric NPs at various polymer concentrations and MWs —the assembly of some of them being significantly difficult by 2D HFF or bulk nanoprecipitation. Optimal ranges of operational parameters are predicted by mathematical modeling and geometric dimensions of channels and inlet holes are fine-tuned by finite element simulations to ensure that the polymer stream is sufficiently exposed to the anti-solvent (water) stream but is not in touch with channel walls. Using confocal microscopy, we further confirm the presence, the position and the shape of the 3D focused polymer stream, which is important for optimal nanoprecipitation of polymeric NPs.

Figure 1a shows a schematic of our 3D focusing channel design for polymeric NP synthesis. The polymer flow (Inlet B) containing polymer precursors dissolved in ACN is

first vertically focused by two vertical ACN sheath flows (Inlet A and C). The vertically arranged stream is subsequently focused horizontally by the water sheath streams and the resulting solvent exchange induces self-assembly of the nanoparticles. Thus, 3D focusing enables isolation of the precipitating polymer from the channel walls. Using this microfluidic device, we synthesized various PLGA-PEG NPs at different polymer precursor concentrations and MWs to investigate the robustness of nanoprecipitation by 3D HFF. In Figure 1b, TEM images of PLGA-PEG NPs made from polymers with various MW and concentrations by 3D HFF show that this method yields fairly monodisperse NPs with a range of sizes.

For comparison between the conventional 2D HFF and 3D HFF, we also constructed 2D HFF channel with identical geometry except for the absence of the two ACN sheath inlets in Figure 1a and we maintained all flow parameters such as net organic stream and water stream flow rates, ensuring similar focused stream geometry and molecular residence time the same for 2D and 3D. When comparing nanoprecipitation using 2D versus 3D HFF (**Figure 2a**), we found that only the 3D HFF method could successfully produce NPs with long-term operation (>10 min) without channel fouling. Polymers with high MWs or high concentrations are usually more susceptible to aggregation in microchannels. Such aggregation during 2D HFF occurred unpredictably at random locations along the channel and thus resulted in poor reproducibility. We also compared the size and monodispersity of NPs synthesized by 3D HFF to 2D HFF and conventional bulk nanoprecipitation for various concentrations (10-50 mg mL^{-1}) and PLGA-PEG MWs (27, 45, and 95 kDa) to verify the quality of NPs prepared by this method (**Figure 2b**). 3D HFF consistently yielded NPs with the smallest size and lowest polydispersity while 2D HFF and bulk method sometimes produced distinctly larger NPs, or failed to produce NPs at all. NP synthesis by 2D HFF was impossible for high MW and high concentration cases due to device failure caused by aggregation. **Figure 2c** shows a comparison of the size distributions of NPs made from $PLGA_{95K}$-PEG_{5K} precursors at low and high concentrations (10 mg mL^{-1} and 50 mg mL^{-1}, respectively) using the three different methods. At high concentrations, NPs obtained by 2D HFF and bulk method yielded highly polydisperse particles of extremely large size (>1000 nm), while 3D HFF consistently resulted in smaller NPs with relatively low polydispersity regardless of polymer concentrations. These observations indicate that 2D HFF is comparable with 3D HFF only for small MW polymers or very low polymer concentrations where the channels are less susceptible to fouling. Consequently, 3D HFF is the only method that enables the reproducible synthesis of monodisperse NPs made from different PLGA MWs and at different concentrations with average NP sizes ranging from 30 to 230 nm.

To identify conditions that enable robust nanoprecipitation in our 3D HFF device, we assembled pure poly(lactic-co-glycolic acid) (PLGA) NPs that are especially prone to aggregation due to the absence of the protective hydrophilic PEG chain as an extreme case model of PLGA-PEG NPs without the PEG shell. Since the flow velocity is slow before horizontal focusing by the water streams, diffusion of the vertically focused polymer stream to the walls must be minimized to prevent isolation. We used a mathematical model to predict optimal parameter ranges for reproducible synthesis of PLGA NPs without aggregation. These parameters collectively define two phases to which the synthesis conditions correspond; the conditions where good and predictable NPs are synthesized in the microfluidic rapid mixing environment without aggregation (Phase I, Good NPs) and the conditions where aggregation occurs (Phase II, Aggregation) (**Figure 2d**). We expressed the phase space in terms of two parameters: *i*) the fraction of polymer flow rate and *ii*) the modified *Péclet* number (*Pe**). First, as the fraction of polymer flow rate in total organic (polymer + ACN) flow rate (*f*) increases, the vertical sheath layer becomes thinner, and eventually the focusing profile approaches to 2D HFF (*f*=1 for 2D HFF), where the system is

more susceptible to aggregation . Second, *Pe**, defined as a product of the *Péclet* number (u_{max}·*h/D*, where u_{max} is the maximal flow velocity and *D* is the diffusion coefficient of polymer precursors in ACN) and the ratio of channel height to focusing length (*h/L*), takes into account the relative importance of convection to diffusion of the polymer precursor. The solid green line in Figure 2d represents conditions where the focusing *Péclet* number, Pe_f=(1/3)**Pe**·(1-*f*)^2, is 10, which indicates that axial convection effectively dominates over lateral diffusion. This dimensionless number not only describes the ratio of diffusive and convective timescales but accounts for thickness of the sheath layer during flow focusing. For low *Pe**, precursor molecules in the focused stream rapidly diffuse from the center to the channel wall. We then expect significant concentration of polymer at the wall, invalidating vertical focusing. The condition where Pe_f=10 thus serves as a suggested boundary line between Phasse I and II. The polymer precursor concentration near the walls acts as a critical determinant of aggregation. Based on the empirical observations that aggregation occurred only when the polymer concentration exceeded a certain threshold (in case of 2D HFF), we defined a critical wall concentration (1 mg/mL for $PLGA_{70K}$) for 3D HFF, above which aggregation may be expected. Conditions under which a wall concentration of 1 mg/mL is obtained from mathematical modeling (dashed red line in Figure 2d) agree qualitatively with the line corresponding to Pe_f=10, as is expected for the polymer concentration used in experiments. Consequently, Figure 2d shows good agreement between experimental data and the calculated phase diagram. These results suggest that diffusion of polymers into the vertical sheath flows, governed by the polymer flow ratio (*f*) and the modified *Péclet* number can explain regimes where the 3D HFF device can successfully isolate the precipitating polymers from the channel walls and operate without aggregation. Thus, we can mathematically predict optimal operating conditions in our system that result in robust nanoprecipitation of NPs and prevent fouling of the microchannel (For detailed discussion about mathematical modeling and analysis, see the supporting information).

To elucidate the effect of inlet hole geometry on device performance, we performed finite element simulations using COMSOL. The aspect ratio (width to height, *w/h*) of the channel where vertical focusing occurs and the size and position of inlet holes are particularly important design factors since they determine the shape of 3D focusing in the channel. The simulations showed a strong influence of the aspect ratio *(w/h)* on the distribution of the polymer after vertical focusing (**Figure 3a**). For the deep channel with *w/h* < 2, vertical lamination successfully occurred with a flat concentration profile, whereas the channel with *w/h* > 2 resulted in a ‘banana-like’ profile with long tails extending to the top wall, making this configuration more susceptible to aggregation. The inlet hole diameter was also found to significantly influence the concentration profile (**Figure 3b**) and the most uniform vertical focusing was obtained for hole sizes slightly larger than the channel width. Smaller holes significantly compromised vertical focusing, again resulting in a ‘banana-like’ polymer stream profile. Likewise, the lateral position of inlet holes affected the shape of vertically focused polymer stream. Off-centered inlets resulted in a tilted polymer stream (**Figure 3c**), which invalidates vertical focusing since precipitating polymer would touch the channel wall. These simulations show that the best 3D focusing is obtained using deep, high aspect ratio channels with well-centered holes of diameters slightly larger than the channel width. Finally, we used confocal microscopy to verify the performance of 3D HFF by three sequential inlets. We used a FITC (green) labeled stream as the focused stream, and a rhodamine (red) labeled stream as the vertical sheath streams. The results in **Figure 3d** showed vertical and horizontal hydrodynamic focusing with the three-sequential-inlet system. In accordance with simulation results, we observed a biased distribution of the focused flow for off-center holes. Similarly, with an inlet hole size smaller (~150 μm) than the width (~200 μm) of the shallow channel, ‘banana-like’ concentration profiles were observed as predicted with simulations. However, such distortion in polymer distributions

was avoided and successful 3D focusing was obtained with a deep channel (low *w/h*). These observations by confocal microscopy, collectively, are in good agreement with the previous simulations. In summary, we presented a new yet simple method to isolate precipitating precursors in microfluidic channels using 3D hydrodynamic focusing enabled by sequential inlets. This approach was used to synthesize PLGA-PEG and PLGA NPs by nanoprecipitation under conditions where monodisperse NPs could neither be synthesized by 2D HFF nor by bulk mixing in a controlled manner. NPs synthesized by 3D HFF exhibited smaller sizes and improved monodispersity compared to 2D HFF or bulk synthesis, keeping the NP size small enough for optimal uptake (i.e. < 100 nm), which is desired in applications where a high MW PLGA block is needed to obtain a specific release profile or where different hydrophobic polymers are mixed.[32-34] More importantly, the monodispersity of the 3D HFF enables the fine-tuning of NP size by carefully choosing PLGA block size of the polymer and the concentration in ACN. Mathematical modeling, together with simulations and confocal microscopy verified the design validity for the performance of the device and defined optimal device geometry and operating conditions for robust 3D HFF. This simple yet versatile design can be easily adapted to microfluidic reactors for synthesis of various materials where isolation of precipitating or reacting flow streams is desirable to prevent fouling and increase robustness during operation.[31, 35-37]

Experimental

Experimental Subheading

Experimental Details. 12 point, double-spaced. References are not superscripted and appear before punctuation [6].

[CCDC nnnnnn contains the supplementary crystallographic data for this paper. These data can be obtained free of charge from The Cambridge Crystallographic Data Centre via www.ccdc.cam.ac.uk/data_request/cif.] ((delete if not applicable))

[Further details of the crystal structure investigation(s) may be obtained from the Fachinformationszentrum Karlsruhe, 76344 Eggenstein-Leopoldshafen (Germany), on quoting the depository number CSD-...] ((delete if not applicable))

((Physical data should be quoted with decimal points and negative exponents (e.g. 25.8 J K^{-1} mol^{-1}), and arranged as follows where possible: mp/bp 20 °C; $[\alpha]_D^{20} = -13.5$ (c = 0.2 in acetone) (please also give units for [α] and c, usually deg cm^3 g^{-1} dm^{-1} and gcm^{-3}, respectively); ^{1}H NMR (400 MHz, DMSO-d_6, δ): 7.15 (s, 2H, Ar H), 1.3 (q, J = 8 Hz, 2H; CH_2), 0.9 (t, J = 8 Hz, 3H; CH_3); ^{13}C NMR (100 MHz, $CDCl_3$, δ): 175.4 (C=O), 156.5 (C4); IR (KBr): ν = 2972 (w), 2907 (w), ..., 1026 (s; ν_{as}(SiOSi)), 971 (vs), ..., 666 (w; ν_s(SiOSi)), ..., 439 (m), 401 cm^{-1} (m); UV-vis (n-hexane): λ_{max} (ε) = 320 (5000), 270 nm (12000); EIMS (m/z (%)): 108 (20) [M^+], 107 (60) [$M^+ - H$], 91 (100) [$C_7H_7^+$]; HRMS (ESI, m/z): $[M + H]^+$ calcd for $C_{21}H_{38}N_4O_6S$, 475.2591; found, 475.2593. Anal. calcd for $C_{45}H_{28}N_4O_7$: C 62.47, H 3.41, N 6.78; found: C 62.27, H 3.46, N 6.80.))

Supplementary Material

Refer to Web version on PubMed Central for supplementary material.

Acknowledgments

This research was supported by the Koch-Prostate Cancer Foundation Award in Nanotherapeutics (R.L. and O.C.F.), by the Concept Development Grant 5P50CA090381-09 from the Dana Farber Cancer Institute Prostate SPORE (O.C.F.), and by NIH Grants CA119349 (R.L. and O.C.F.) and EB003647 (O.C.F.). We thank Jongho Lee

(MIT), Mikhail Hanewich-Hollatz (MIT) and Fawziya Z. Karim (MIT) for their assistance in experiments. We also appreciate valuable discussions on mathematical analysis with Soyeon Lee (Indiana University).

References

1. Soppimatha KS, Aminabhavi TM, Kulkarnia AR, Rudzinski WE. J. Controlled Release. 2001; 70:1.
2. Peer D, Karp JM, Hong S, Farokhzad OC, Margalit R, Langer R. Nat. Nanotechnol. 2007; 2:751. [PubMed: 18654426]
3. Davis ME, Chen ZG, Shin DM. Nat. Rev. Drug. Discov. 2008; 7:771. [PubMed: 18758474]
4. Riehemann K, Schneider SW, Luger TA, Godin B, Ferrari M, Fuchs H. Angew Chem Int. Ed. Engl. 2009; 48:872. [PubMed: 19142939]
5. Gref R, Minamitake Y, Peracchia MT, Trubetskoy V, Torchilin V, Langer R. Science. 1994; 263:1600. [PubMed: 8128245]
6. Farokhzad OC, Langer R. ACS Nano. 2009; 3:16. [PubMed: 19206243]
7. Farokhzad OC, Cheng J, Teply BA, Sherifi I I, Jon S, Kantoff PW, Richie JP, Langer R. Proc. Natl. Acad. Sci. USA. 2006; 103:6315. [PubMed: 16606824]
8. Farokhzad OC, Jon S, Khademhosseini A, Tran TN, Lavan DA, Langer R. Cancer Res. 2004; 64:7668. [PubMed: 15520166]
9. Gu F, Zhang L, Teply BA, Mann N, Wang A, Radovic-Moreno AF, Langer R, Farokhzad OC. Proc. Natl. Acad. Sci. U S A. 2008; 105:2586. [PubMed: 18272481]
10. Murday JS, Siegel RW, Stein J, Wright JF. Nanomedicine. 2009; 5:251. [PubMed: 19540359]
11. Cheng J, Teply BA, Sherifi I, Sung J, Luther G, Gu FX, Levy-Nissenbaum E, Radovic-Moreno AF, Langer R, Farokhzad OC. Biomaterials. 2007; 28:869. [PubMed: 17055572]
12. Avgoustakis K. Curr. Drug Deliv. 2004; 1:321. [PubMed: 16305394]
13. Karnik R, Gu F, Basto P, Cannizzaro C, Dean L, Kyei-Manu W, Langer R, Farokhzad OC. Nano Lett. 2008; 8:2906. [PubMed: 18656990]
14. Valencia PM, Basto PA, Zhang L, Rhee M, Langer R, Farokhzad OC, Karnik R. ACS Nano. 2010; 4:1671. [PubMed: 20166699]
15. Johnson BK, Prud'homme RK. Phys. Rev. Lett. 2003; 91:118302. [PubMed: 14525460]
16. Wong I, Ho CM. Microfluid Nanofluid. 2009; 7:291. [PubMed: 20357909]
17. Wu D, Luo Y, Zhou X, Dai Z, Lin B. Electrophoresis. 2005; 26:211. [PubMed: 15624173]
18. Govender T, Riley T, Ehtezazi T, Garnett MC, Stolnik S, Illum L, Davis SS. Int. J. Pharm. 2000; 199:95. [PubMed: 10794931]
19. Riley T, Stolnik S, Heald CR, Xiong CD, Garnett MC, Illum L, Davis SS, Purkiss SC, Barlow RJ, Gellert PR. Langmuir. 2001; 17:3168.
20. Chan EM, Alivisatos AP, Mathies RA. J. Am. Chem.Soc. 2005; 127:13854. [PubMed: 16201806]
21. Rolland JP, Van Dam RM, Schorzman DA, Quake SR, DeSimone JM. J. Am. Chem. Soc. 2004; 126:2322. [PubMed: 14982433]
22. Yanga R, Feeback DL, Wanga W. Sensor Actuat. A. 2005; 118:259.
23. Huang S, Tan W, Tseng F, Takeuchi S. J. Micromech. Microeng. 2006; 16:2336.
24. Wolff A, Perch-Nielsen IR, Larsen UD, Friis P, Goranovic G, Poulsen CR, Kuttera JP, Telleman P. Lab Chip. 2003; 3:22. [PubMed: 15100801]
25. Mao X, Waldeisen JR, Huang TJ. Lab Chip. 2007; 7:1260. [PubMed: 17896008]
26. Lim J-M, Kim S-H, Yang S-M. Microfluid. Nanofluid. 2010 DOI 10.1007/s10404-010-0649-5.
27. Simonnet C, Groisman A. Appl. Phys. Lett. 2005; 87:114104.
28. Scott R, Sethu P, Harnett CK. Rev. Sci. Instrum. 2008; 79:046104. [PubMed: 18447562]
29. Kim DS, Kim DS, Han K, Yang W. Microelectron. Eng. 2009; 86:1343.
30. Chang C-C, Huang Z-X, Yang R-J. J. Micromech. Microeng. 2007; 17:1479.
31. Bong KW, Bong KT, Pregibon DC, Doyle PS. Angew. Chem. Int. Ed. 2010; 49:87.
32. Jiang W, Kim BY, Rutka JT, Chan WC. Nat. Nanotechnol. 2008; 3:145. [PubMed: 18654486]
33. Beletsi A, Panagi Z, Avgoustakis K. Int. J. Pharm. 2005; 298:233. [PubMed: 15936907]
34. Cho H-K, Cheong I-W, Lee J-M, Kim J-H. Korean J. Chem. Eng. 2010; 27:731.

35. Takayama S, Ostuni E, LeDuc PR, Naruse K, Ingber DE, Whitesides GM. Nature. 2001; 411:1016. [PubMed: 11429594]

36. Dittrich PS, Schwille P. Anal. Chem. 2003; 75:5767. [PubMed: 14588016]

37. de Mello AJ, Edel JB. J. Appl. Phys. 2007; 101:084903.

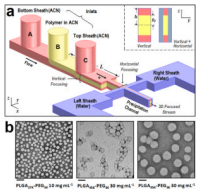

Figure 1.

(a) Concept of device for 3D hydrodynamic focusing (not to scale) consisting of three sequential inlets for vertical focusing and a separate inlet for side sheath flows (not shown). The cross-sectional views in the inset show the vertically focused stream profile (left) and the heterogeneous 3D hydrodynamic focusing where the sample flow is isolated both horizontally and vertically (right). (b) TEM images of PLGA-PEG NPs obtained from $PLGA_{27K}$-PEG_{5K} at 10 mg mL^{-1} in ACN (scale bar 100 nm), $PLGA_{45K}$-PEG_{5K} at 30 mg mL^{-1} in ACN (scale bar 100 nm) and $PLGA_{95K}$-PEG_{5K} at 30 mg mL^{-1} in ACN (scale bar 200 nm) using 3D HFF with the flow ratio of Polymer:ACN = 3:7 and organic:water = 1:5. Average NP sizes are 33.8, 55.0, and 200 nm, respectively.

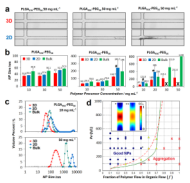

Figure 2.

Comparison of 3D HFF (f = 0.3), 2D HFF, and bulk nanoprecipitation of PLGA-PEG NPs under different conditions with the flow ratio of organic:water = 1:10. (a) Representative channel images of the device during synthesis of PLGA-PEG NPS by 3D HFF and 2D HFF for various MW precursors, showing aggregation in the case of 2D HFF. All micrographs were captured after ~500 s of operation (channel width 20 μm). (b) Effect of the PLGA-PEG precursor concentration on the final NP sizes depending on the MW of the precursors and the choice of a synthesis method. **X** = Clogging of channel within 3 minutes of operation. * = Aggregation of polymer in channel observed after 5-10 minutes of operation. # = Aggregation of polymer in channel observed after >10 minutes of operation. (c) Size distributions by volume fraction of $PLGA_{95K}$-PEG_{5K} NPs prepared by microfluidic 3D HFF, 2D, and bulk mixing methods for the precursor concentrations of 10 and 50 mg/mL, respectively. Aggregated particles are found in the 1,000-10,000 nm range. (d) Phase space of 3D HFF operation parameters (Pe* and f) for synthesis of PLGA NPs from pure $PLGA_{70K}$ precursors (10 mg mL^{-1}). Solid green line represents condisitons where Pe_f*=10 and dashed red line represents conditions under which the $PLGA_{70K}$ precursor reaches a critical wall concentration (1 mg mL^{-1}) that results in aggregation. Both lines delineate conditions that result good synthesis of NPs (Phase I) from those that are susceptible to aggregation (Phase II). Symbols indicate experimental data for the synthesis of $PLGA_{70K}$ NPs. (O: reproducible, successful NP synthesis, X: aggregation with microparticle formation, Δ: mild or occasional aggregation). Inset shows simulated concentration profiles at the starting poirnt of nanoprecipitation under the conditions where flow rates (u_{max}) are different but f is the same for Phase I (*) and Phase II (**), respectively.

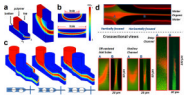

Figure 3.

(a) 3D simulations with different channel aspect ratios (*w/h*); 3.33 (left) and 0.83 (right), respectively. Perspective views of the channel with the width of 200 μm and the inlet of 150 μm. Only the left halves about the symmetry plane are shown. (b) Simulated cross-sectional views for two different inlet hole diameters at a fixed channel aspect ratio (*w/h* = 3.33). (c) 3D simulations for a channel of *w* = 100 μm and *h* = 100 μm, showing off–centered inlet (left), well aligned inlet (center), and slightly larger inlet (right). (d) Confocal micrographs showing cross-sectional views of vertical focusing before (A) and after (B) horizontal focusing. The top panel shows a top-view of the system near the lateral squeezing cross juction. In the bottom left panel, off-centered holes directly compare with the left panel in (c). The bottom center panel shows vertical focusing occurred in the channel of *w/h* = 3.33 while the sequential inlet hole size was slightly smaller. The bottom right panel shows vertical focusing occurred in the channel of *w/h* = 1.0.